Structure Property Analysis of the Solution and Solid-State Properties of Bistable Photochromic Hydrazones

Baihao Shao,† Hai Qian,† Quan Li, Ivan Aprahamian*

Department of Chemistry, Dartmouth College, Hanover, New Hampshire 03755, USA.

KEYWORDS. Hydrazones, photochromic compounds, bistability, emission toggling, molecular switches

ABSTRACT: The development of new photochromic compounds, and the optimization of their photophysical and switching properties are prerequisites for accessing new functions and opportunities that are not possible with currently available systems. To this end we recently developed a new bistable hydrazone switch that undergoes efficient photoswitching and emission ON/OFF toggling in both solution and solid-state. Here, we present a systematic structure-property analysis using a family of hydrazones, and show how their properties, including activation wavelengths, photostationary states (PSSs), photoisomerization quantum yields, thermal half-lives ($\tau_{1/2}$), and solution/solid-state fluorescence characteristics vary as a function of electron donating (EDG) and/or withdrawing (EWG) substituents. These studies resulted in the red-shifting of the absorption profiles of the *Z* and *E* isomers of the switches, while maintaining excellent PSSs in almost all of the compounds. The introduction of *para*-NMe_2, and/or *para*-NO_2 groups improved the photoisomerization quantum yields, and the extremely long thermal half-lives (tens to thousands of years) were maintained in most cases, even in a push-pull system, which can be activated solely with visible light. Hydrazones bearing EDGs at the stator phenyl group are an exception and show up to 6 orders of magnitude acceleration in $\tau_{1/2}$ (*i.e.*, days) because of a change in the isomerization mechanism. Moreover, we discovered that a *para*-NMe_2 group is required to have reasonable fluorescence quantum yields in solution, and that rigidification enhances the emission in the solid-state. Finally, X-ray crystallography analysis showed that the switching process is more efficient in the solid-state when the hydrazone is loosely packed.

INTRODUCTION

Photochromic compounds,[1] may they be azobenzenes,[2] stilbenes,[3] spiropyrans,[4] or diphenylethenes[5] form an integral part of the tool-set available to molecular machinists.[6] Throughout the decades, these triggers enabled practitioners to design adaptive materials,[7] and develop drugs,[8] catalysts,[9] artificial molecular machines and motors,[10] in addition to other systems that can be turned ON/OFF using the high spatial and temporal resolution of light. Accessing these functions necessitated the optimization of the properties and capabilities (*e.g.*, photostationary states (PSSs), quantum yields (Φ), thermal relaxation half-lives ($\tau_{1/2}$), absorption/activation wavelengths, emission toggling, etc.) of these light switches, which in turn greatly enhanced the proliferation of these tools in diverse areas of research. Nonetheless, there is yet a need to pinpoint a system and/or families of switches that encompasses all the desirable characteristics of photochromic compounds, *i.e.*, ease of synthesize, high thermal stability, efficient photoconversion, high photostability, broad and tunable activation wavelengths, switching in both solution and solid-state, large geometrical and dipole changes, biocompatibility, switching in aqueous media and serum, resistance to glutathione reduction, *etc*. Driven by a desire to overcome these obstacles, and the onset of new applications and possibilities, such as photopharmacology,[8] the past decade witnessed a surge in the design of new photochromic scaffolds, including but not limited to indigoids,[11] hydrazones,[12] acylhydrazones,[13] azo-BF_2 complexes,[14] heterophenyl azo dyes,[15] imidazole dimers,[16] and donor-acceptor stenhouse adducts.[17] These systems expand the tool-kit available to the scientific community, and will open the way for new opportunities, once their properties are well-understood and optimized.

Scheme 1. The structures of the photochromic hydrazone switches. Rotor and stator designations are arbitrary.

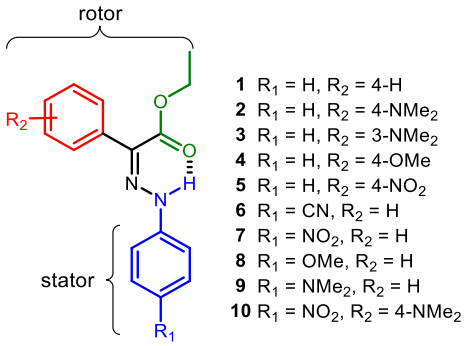

Our interest in developing hydrazone-based molecular switches[18] recently led us to the discovery of a new family of hydrazone-based bistable photochromic switches having half-lives ($\tau_{1/2}$) as long as 5,300 years.[19] We subsequently used these switches in polymer actuation,[20] and controlling the self-assembly of liquid-crystals.[21] In both these instances the bistability of the switch gave us access to hitherto underexplored properties – multistep/state actuation and order to higher order phase transitions (*i.e.*, from cholesteric to Smectic A) – thus showcasing the benefits of designing new switchable systems. Next, we showed that substituting the stator phenyl moiety with a *para*-dimethyl amine (NMe_2) group (**2**) yields an emissive compound whose fluorescence could be toggled 'ON' and 'OFF' both in the solution and solid-state.[22] Herein, we report on a systematic study of the solution and solid-state switching and fluorescence emission properties of this new class of photoswitches. The structure property analyses (Scheme 1) were conducted by derivatizing the rotor (red) and stator (blue) phenyl groups with electron-withdrawing (EWGs) and electron-donating groups (EDGs). These modifications allowed us to assess the substituent effect on the photostationary states and quantum yields of the switch, tune the half-life from thousands of years to days, and red-shift the activation (Figure 1) and emission wavelengths of the hydrazones. Moreover, we made strides in showing that emission in these systems indeed stems from excited-state intramolecular proton transfer (ESIPT)-coupled charge transfer (CT). Finally, analysis of X-ray data corroborated the hypothesis that loose packing is responsible for both the switching of the systems and their emission in the solid-state.

RESULTS AND DISCUSSION

Synthesis: Hydrazones **3**, **4**, **6**, **7**, **8** and **10** were synthesized in good yields (52-83%) using a facile one-step procedure starting from appropriately substituted hydrazines and α-ketoesters (Scheme S1 in the Supporting Information). Hydrazones **1**[19a] and **2**[22] were synthesized in a similar manner and used as reference compounds. While, compounds **5** and **9** were prepared (49 and 78%, respectively) using a one-step diazo coupling reaction (Scheme S2 in the Supporting Information). The *Z* isomer was separated (after column chromatography) as the major configurational isomer in all reactions. This assignment was corroborated using the chemical shift of the intramolecular H-bond between the NH proton and carbonyl oxygen that resonates between 11.5 – 13.0 ppm in toluene-d_8. All the new compounds were fully characterized using NMR spectroscopy, high-resolution mass spectrometry, and X-ray crystallography (See Figures S1–16 and S74–80 in the Supporting Information).

Photophysical Properties: The UV spectra of the *Z* and *E* isomers (obtained after irradiation at appropriate wavelength or by data extrapolation) of compounds **3-10** were measured (or derived) in toluene. We will first focus our discussion on the EWG containing derivatives. The absorption maxima (λ_{max}) of the *Z* and *E* forms of the *para*-CN substituted hydrazone **6** are almost identical to those of **1** (Table 1). Conversely, *para*-NO_2 substitution on either the rotor (**5**) or stator (**7**) phenyl ring induces a *ca.* 20 nm red-shift in the λ_{max} of the *Z* isomers. This unusual effect could be attributed to the formation of a "quinoid" form in **7** which leads to the extension of the π-system through resonance between the hydrazone NH nitrogen and the NO_2 group,[23] and a more stabilized LUMO (*i.e.*, narrower HOMO-LUMO gap) in **5**. The red-shift (33 nm) is retained in the *E* isomer of **7** relative to **1** as the effect stems from the stator part, which is not effected by isomerization, while a 20 nm blue-shift is observed in **5**-*E*, which is the expected outcome upon NO_2-substitution, and loss of H-bonding induced planarity of hydrazone skeleton. All three hydrazones have excellent PSSs (>90%; 410/442 nm irradiation) going from *Z* to *E* (Table 1), thanks to the well-separated absorption bands of the two isomers (Figure 2b, Figures S23 and S26 in the Supporting Information). The PSSs for the reverse process are also very high (> 80%; 340/365 nm irradiation) for compounds **6** and **7**, while for **5** a PSS_{340} of 52% was measured because irradiation was done very close to the isosbestic point.[24] Good quantum yields (>10%) were measured for both isomerization directions in **5** and **7**, and particularly high (35.3%) for the $Z \rightarrow E$ isomerization process in **7**. Compound **6** on the other hand exhibits lower Φ values ($\Phi_{Z\rightarrow E}$ = 4.1 ± 0.1% and $\Phi_{E\rightarrow Z}$ = 5.1 ± 0.3%). All three compounds exhibit good fatigue resistance as well (Figure 2c and Figures S24 and S27).

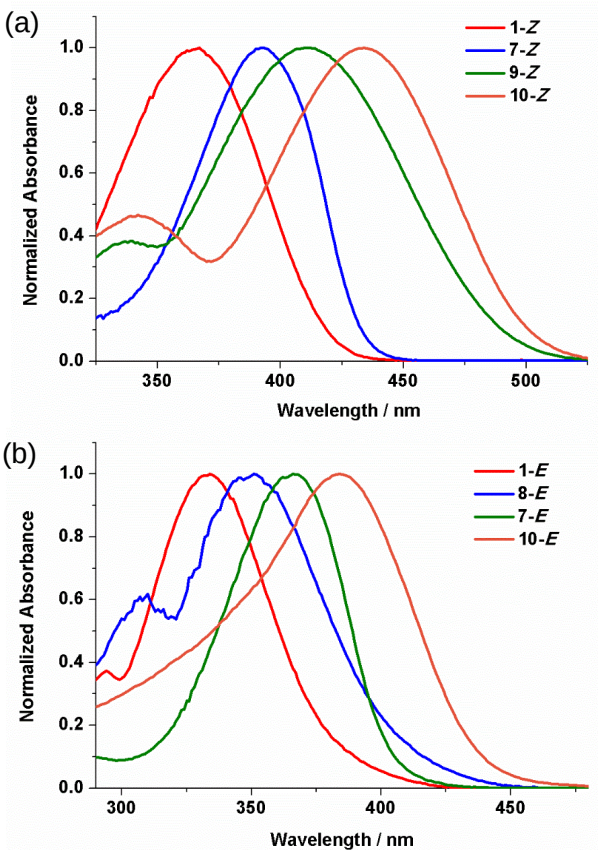

Figure 1. (a) Normalized UV-Vis spectra for the *Z* isomers of hydrazones **1**, **7**, **9** and **10** in toluene; (b) Normalized UV-Vis spectra for the *E* isomers of hydrazones **1**, **7**, **8** and **10** in toluene.

Table 1. Photophysical data for compounds 1–10 in toluene.

Hydrazone	λ_{max} (nm) / ε^a		Φ		PSS @ λ_{irr} (nm)	
	Z	*E*	*Z*→*E*	*E*→*Z*		
1[b]	367 / 18300	334 / 18000	7.5 ± 0.1 %	10.6 ± 0.2 %	95 % of *E* @ 410	76 % of *Z* @ 340
2[c]	395 / 14500	343 / 13800	32.0 ± 0.9 %	14.7 ± 1.0 %	> 99 % of *E* @ 442	82 % of *Z* @ 340
3	366 / 19200	331 / 19300	16.2 ± 0.5 %	10.7 ± 0.5 %	> 99 % of *E* @ 410	54 % of *Z* @ 340[d]
4	376 / 21100	330 / 19500	4.7 ± 0.1 %	9.1 ± 0.6 %	98 % of *E* @ 410	84 % of *Z* @ 340
5	392 / 24900	314 / 13500	11.7 ± 0.3 %	12.6 ± 1.3 %	92 % of *E* @ 442	52 % of *Z* @ 340[d]
6	368 / 26300	333 / 26600	4.1 ± 0.1 %	5.1 ± 0.3 %	> 99 % of *E* @ 410	86 % of *Z* @ 340
7	391 / 26800	366 / 24300	35.3 ± 2.1 %	11.4 ± 0.1 %	98 % of *E* @ 442	82 % of *Z* @ 365
8	383 / 17200	351 / 13900	5.3 ± 0.1 %	9.5 ± 0.5 %	93 % of *E* @ 442	88 % of *Z* @ 340
9	410 / 17800	398 / 11900	65.4 ± 6.1 %	-[e]	27 % of *E* @ 480	-[e]
10	435 / 18300	384 / 17600	46.2 ± 4.2 %	7.4 ± 1.1 %[f]	> 99 % of *E* @ 480	96 % of *Z* @ 375[f]

[a] The extinction coefficient (ε) is calculated in L mol^{-1} cm^{-1}; [b] Ref 19a; [c] Ref 22; [d] Band overlap and hence no access to optimal switching wavelength; [e] Because of the poor band separation, an optimal irradiation wavelength was not found to initiate the *E*→*Z* isomerization process; [f] Φ = 19.4 ± 0.6 % and PSS = 90 % of *Z* when 410 nm light is used for the *E* → *Z* process.

Hydrazones **4**, **8** and **9**, having EDGs at the *para*-position of the stator or rotor phenyl groups all show a red-shift in the λ_{max} of their *Z* isomer relative to **1**, which also holds for the *E* isomer of **8** and **9** (Table 1). Compounds **4** and **8** also show excellent PSSs (84%-98%) and moderate Φ values (4.7%-9.5%). Switch **9** exhibits the largest bathochromic shifts in both the *Z* (42 nm) and *E* (64 nm) forms, compared with **1**, and the highest $\Phi_{Z\rightarrow E}$ (65.4 ± 6.1%) among all switches. Unfortunately the overlap between the *E* and *Z* absorption bands (Figure S35 in the Supporting Information) resulted in a low PSS for the *Z*→*E* process (Figure S36 in the Supporting Information). The red-shifts observed in **9** results from the strong ED nature of *para*-NMe_2 and the conjugation of the stator phenyl ring with the hydrazone core.

Next, we synthesized the push-pull switch **10** to combine the promising properties obtained when having a *para*-NO_2 group at the rotor, and *para*-NMe_2 group at the stator phenyl groups. The λ_{max} of **10**-*Z* is red-shifted by 68 nm (to 435 nm) relative to hydrazone **1** (Figure S37 in the Supporting Information). Upon irradiation with 480 nm light, a PSS_{480} of > 99 % *E* is obtained (Figure S40b in the Supporting Information). The quantum yield of the process is significantly higher ($\Phi_{Z\rightarrow E}$ = 46.2 ± 4.2 %) relative to the other derivatives. The **10**-*E* absorption band is bathochromically shifted by 50 nm (λ_{max} = 384 nm) relative to **1**. The back photoisomerization of **10**-*E* is achieved using 375 nm light source to afford a PSS_{375} of 96% *Z* (Figure S40c in the Supporting Information) with $\Phi_{E\rightarrow Z}$ = 7.4 ± 1.1 %. Moreover, the *E*→*Z* isomerization process can be driven using 410 nm light (PSS_{410} of 90% *Z*, $\Phi_{E\rightarrow Z}$ = 19.4 ± 0.6 %) making **10** the first member of the hydrazone photochromic family that can be solely switched with visible light (Figure S41 in the Supporting Information). These results indicate that the push-pull design strategy is a viable one for red-shifting the absorption band of the hydrazone switches.

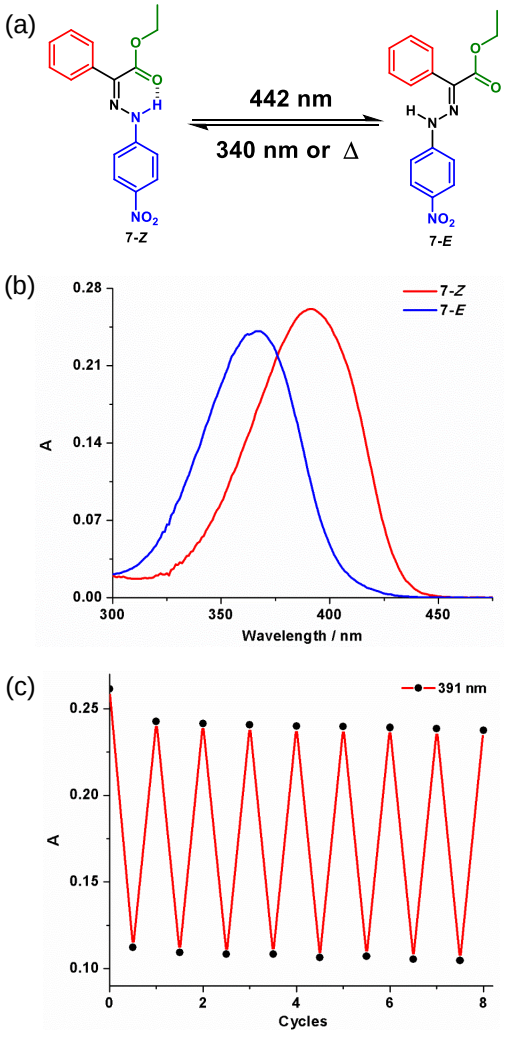

Figure 2. (a) Light-activated photoisomerization of hydrazone **7**; (b) UV-Vis spectra (1×10^{-5} M) of **7**-*Z* and **7**-*E* isomers in toluene; (c) Photoswitching cycles of **7** in toluene upon alternating the irradiation wavelength between 442 and 340 nm light.

Scheme 2. The proposed conjugation in 5, 8, and 9 that accelerates the isomerization process.

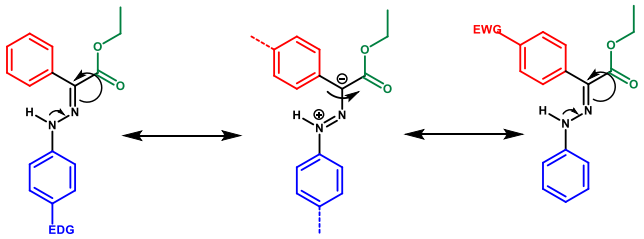

Kinetic Properties: The thermal isomerization rates of the photochromic hydrazones were measured (in most cases) at an elevated temperature (368K) and the data were extrapolated to room temperature using the Arrhenius and Eyring equations to yield $\tau_{1/2}$ and activation barriers, respectively (Figure S58–65 in the Supporting Information). The extremely long thermal half-lives (year scale) are retained in most of the compounds, except for the ones with EDGs at the stator phenyl group (*i.e.*, **8** and **9**), where the rate is accelerated by up to 6 orders of magnitude relative to **1**. We hypothesize that the extended conjugation in these two systems (Scheme 2) imparts a partial single bond character to the C=N double bond, which in turn facilitates the isomerization process. That is, in **8** and **9** the isomerization mechanism is no longer inversion as in the rest of the family, but rather rotation around the imine bond. Analysis of the X-ray structures of **6**-**9** (*Z*-isomers because not enough crystals of the *E*-isomers were obtained) corroborates this hypothesis as the C=N bond is longer in **8** and **9** (1.310 and 1.317 Å, respectively) relative to **6** and **7** (1.304 and 1.299 Å), while the N–N single bond is shorter (1.323 and 1.322 Å for **8** and **9**, respectively, *vs.* 1.334 and 1.342 Å for **6** and **7**, respectively).

Table 2. Kinetic data for the thermal isomerization of compounds 1–10 in toluene at 298 K.

Hydrazone[a]	k^b / s^{-1}	$\tau_{1/2}{}^c$ / year	$\Delta G^{\ddagger d}$ / kcal·mol^{-1}
1[e]	$(6.8 \pm 0.2) \times 10^{-11}$	324 ± 11	31.5 ± 0.1
2[f]	$(1.0 \pm 0.1) \times 10^{-10}$	213 ± 7	31.2 ± 0.1
3	$(1.3 \pm 0.1) \times 10^{-11}$	1645 ± 33	32.5 ± 0.1
4	$(3.3 \pm 0.2) \times 10^{-11}$	664 ± 44	32.0 ± 0.2
5	$(1.1 \pm 0.2) \times 10^{-9}$	20 ± 3	29.8 ± 0.1
6	$(2.1 \pm 0.1) \times 10^{-11}$	1033 ± 52	32.2 ± 0.1
7	$(1.7 \pm 0.1) \times 10^{-11}$	1286 ± 28	32.3 ± 0.1
8	$(5.6 \pm 0.2) \times 10^{-7}$	0.039 ± 0.002[g]	26.0 ± 0.1
9	$(1.5 \pm 0.1) \times 10^{-5}$	0.0015 ± 0.0001[g]	24.0 ± 0.1
10	$(1.8 \pm 0.2) \times 10^{-10}$	126 ± 11	30.9 ± 0.1

[a] Thermal relaxation occurs from $E \rightarrow Z$; [b] The 1st-order rate constants at 298 K were calculated using the Arrhenius equation; [c] Half-life at 298 K; [d] The Gibbs energy of activation was determined using the Eyring equation; [e] Ref 19a; [f] Ref 22; [g] The kinetic study was performed at room temperature.

Substitution at the rotor phenyl ring has a less significant effect, in general, on the thermal relaxation rates, and the half-lives are either slightly increased (**3, 4**) or decreased (**2**) relative to **1**. One exception is **5** where a 2 order of magnitude acceleration in rate is measured. This observation can be explained by the conjugation between the hydrazone NH nitrogen and the nitro group, which imparts a partial single bond character to the C=N double bond (Scheme 2). The X-ray structure of **5** supports this hypothesis as the C=N double bond (1.319 Å) and N–N single bond (1.320 Å) are longer and shorter, respectively, than in **6** and **7**, for example. The effect is not as drastic as in **8** or **9** because the rotor phenyl group is not co-planar with the rest of the molecule, and so the conjugation is not as effective. Finally, it is noteworthy that the half-life in **10** is 126 ± 11 years, which is highly unusual for a push-pull system,[2] resulting in a red shift in absorption band while maintaining bistability.

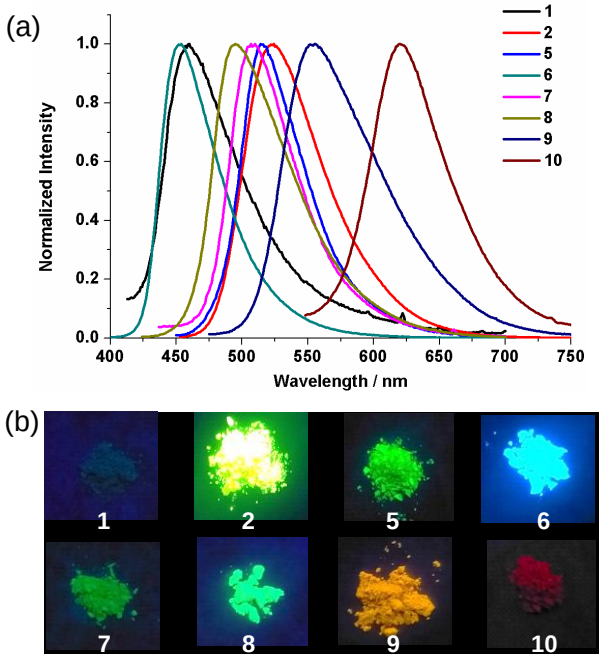

Figure 3. (a) The normalized solid-state fluorescence spectra of **1, 2** and **5-10** powders (the absorption maxima in toluene were chosen as excitation wavelengths for each compound); (b) Fluorescence emissions from the powders of hydrazones **1**, **2** and **5-10** under 365-nm UV lamp.

Solution and Solid-State Fluorescence Properties: The emission properties of hydrazones **3**-**10** were first studied in solution using fluorescence spectroscopy (Table 3). The compounds show emissions with varying intensities in toluene at wavelengths (λ_{em}) ranging from 450 nm to 560 nm (Figure S66 in the Supporting Information). Hydrazones **2**, **4**, **8** and **9** bearing EDGs (-OMe or -NMe_2) exhibit emission at longer wavelengths in general, compared with those bearing electron-withdrawing groups (-CN or -NO_2 groups, i.e., **5**, **6** and **7**). It should be noted that while emission is observed for these compounds in solution its intensity is very low, and so we

Table 3. Summary of photophysical properties of hydrazones 1-10 in solution and solid-state (powder and crystal).

Hydrazone	Solution				Crystal		Powder		
	λ_{max} (nm)	λ_{em} (nm)[a]	Φ (%)	τ (ns)[b]	λ_{em} (nm)[a]	Φ (%)	λ_{em} (nm)[a]	Φ (%)	τ (ps)[b]
1	367	450	-[c]	-	464	-[c]	460	-[c]	-
2[d]	395	525	0.7 ± 0.1	0.19 ± 0.01	520	23.1 ± 0.2	524	27.5 ± 1.4	65 ± 2
3	366	525	-[c]	-	-	-	513	-[c]	-
4[e]	376	475	-[c]	-	-[e]	-[e]	-[e]	-[e]	-
5	392	480	-[c]	-	522	2.9 ± 0.2	514	1.6 ± 0.2	65 ± 1
6	368	456	-[c]	-	457	21.5 ± 0.6	450	19.7 ± 0.5	20 ± 2
7	392	452	-[c]	-	512	-[c]	510	-[c]	-
8	383	498	-[c]	-	500	8.6 ± 0.2	495	6.7 ± 0.1	57 ± 2
9	410	543	-[c]	-	560	0.8 ± 0.1	555	1.0 ± 0.1	65 ± 2
10	435	560	22.6 ± 0.5	2.7 ± 0.1	620	-[c]	620	-[c]	-

[a]Absorption maxima in toluene are used as excitation wavelengths; [b]Fluorescence decay lifetime; [c]Quantum yields are too low to be measured; [d]Ref 22; [e]Hydrazone **4** was obtained as an oil at rt.

could not measure fluorescence quantum yields for most of them. Compound **2** is the most emissive in solution among the mono-substituted hydrazones (Φ_{FL} =0.7 ± 0.1 %), and we previously proposed excited-state intramolecular proton transfer (ESIPT)-coupled charge transfer (CT) as the emission mechanism.[22] In such a mechanism the rotor phenyl group is less twisted relative to the rest of the hydrazone core in the excited state, enhancing the conjugation between the latter and the NMe_2 group.[25] To test this hypothesis we synthesized compound **3** that has the NMe_2 group at the *meta*-position and as expected a drastic quenching of emission was observed (Figure S73 in the Supporting Information). Moreover, the absorption bands of **3** are blue-shifted in both the *Z* (29 nm) and *E* (12 nm) isomers compared to **2** (Table 3) indicating that the conjugation diminishes in the ground state as well. These results validate the role of CT in enhancing hydrazone fluorescence emission and highlight the unique CT capacity of the -NMe_2 group in these systems. As for the "push-pull" switch **10**, it shows relatively strong emission (Φ_{FL} = 22.6 ± 0.5 %) in solution, and has the most red-shifted emission wavelength (560 nm). We postulate that this enhancement in emission results from the presence of the *para*-NO_2 group at the stator phenyl group, which augments the efficiency of the CT process.

Next, we tested the fluorescence emission profiles of hydrazones **1, 3** and **5**-**10** in amorphous (powder) and crystalline states (compound **4** is an oil, and hence, was not including in the analysis). The quantum yield of the strongly emissive **10** decreases dramatically in the solid-state (Table 3) and a large red-shift in emission (~60 nm) is observed, indicating the formation of excimers in the solid-state.[26] The crystal structure of **10** shows compact head-to-tail packing with an interplanar distance of 3.489 Å (Figure 4a and 4b), which we speculate is responsible for the quenching effect. The nitro-substituted compound **7** arranges itself in a similar packing mode (Figure S81 in the Supporting Information) leading to a red-shifted (~60 nm) and very weak emission in the solid-state.

On the other hand, the quantum yields of hydrazones **2** (for comparison), **5**, **6**, **8** and **9** increase in the solid-state (Table 3), giving rise to bright blue to orange fluorescence emission bands (Figure 3b). We speculate that this occurs as a result of rigidification in the solid-state (*e.g.*, aggregation induced emission phenomenon).[27] In contrast with the huge red shifts observed in **7** and **10**, there are no apparent changes in the emission maxima of hydrazones **2**, **6** and **8**, when going from solution to the solid-state. The molecular packing in these systems lends an insight into the disparity between these two groups. For example, two units of **8** are loosely packed in the unit cell (Figure 4c, 4d) with no effective interactions between them leading to the observed photophysical properties. Hydrazones **2** and **6** behave similarly in the solid-state (Figures S82 and S86 in the supporting information).

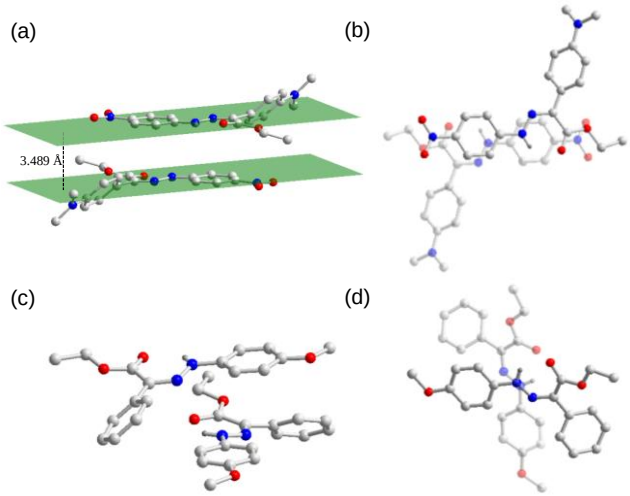

Figure 4. (a) The head-to-tail packing of compound **10** in the crystal structure (the distance between the planes of the hydrazone backbones is shown); (b) The vertical view of the packing motif in **10**; (c) The crystal packing in hydrazone **8**; (d) The orthogonal packing in **8** viewed vertically (C-H protons are omitted for clarity).

Hydrazones **5** and **9** on the other hand show moderate shifts in emission bands and lower quantum yields than **2**, **6** and **8** (Table 3). Again, the crystal structure of these systems helps in understanding this observation. Two molecules of **9** make up the unit cell and stack in a perpendicular fashion where one H-bonded six-membered ring sits on the top of another leading to a cross-shaped pattern (Figure S83 in the supporting information). This loose packing does not lead to complete quenching (quantum yield of ~1%) and only a small red-shift in emission (~15 nm). Hydrazone **5** exhibits a larger bathochromic shift (average of 38 nm) in emission band, and slightly higher quantum yield (~2%). In its crystal structure the rotary phenyl rings of adjacent molecules are located on the same side with a π-π distance of 3.743 Å (Figure S84 in the supporting information). This arrangement might explain the bathochromic shift observed in this system, while the loose packing prevents complete quenching.

Solid-State Photoswitching: In addition to being emissive, some of the hydrazones can also undergo photoisomerization in the solid-state. The switching behavior of drop-casted films of the hydrazones were monitored using UV/Vis spectroscopy. It was found that the process is highly dependent on the packing mode observed in the crystal structures. That is, photoswitching is observed for hydrazones that do not have effective packing of their backbones, which matches the empirical observation that free volume is required in the solid-state for efficient isomerization to take place.[28] For example, compounds **1** and **8** that are orthogonally stacked (*i.e.*, minimum packing of their backbones, see Figure 4c, 4d and Figure S85 in the supporting information) demonstrate highly efficient back-and-forth photoisomerization (Figure S89 and S90 in the Supporting Information). The UV-Vis absorption bands of the *Z* isomers and PSSs for these compounds are similar to the ones measured in toluene, indicating that the same isomerization process is occurring in the solid-state. The absorption bands of **1** and **8** start to broaden and decrease in intensity upon switching cycles, while the peak positions remain unchanged. We ascribe this phenomenon to changes in film morphology (*i.e.*, thickness) [29] upon photoisomerization rather than photodegradation or decomposition. On the other hand, the denser packed **5** and **6** show less efficient switching because of the partial overlap of the hydrazone backbone (Figure S91 and S92 in the Supporting Information). No appreciable switching was observed in tightly packed hydrazones **7** and **10** (Figure S93 and S94 in the Supporting Information). The solid-state emission change in these hydrazones also follows the packing mode. The emission toggling in **5**, **6**, **7** and **10** is not effective because of the low switching efficiency (Figure S91c, S92c, S93c and S94c in the Supporting Information), while in **8** the morphology change in the drop-casted film upon photoswitching diminishes the efficacy of the process (Figure S90c and S90d in the Supporting Information).

CONCLUSIONS

In summary, we systematically studied the effect of ED and EW substituents on the photophysical and switching properties of bistable hydrazone switches. Most derivatives show year-scale thermal half-lives, and good absorption band separation, and hence excellent PSSs, and very good photoisomerization quantum yields. The solution phase studies resulted in the following observations: 1) substituting the hydrazone with *para*-EDGs and *para*-NO_2 group at either the rotor or stator phenyl rings will lead to a red-shift in the absorption profile of the *Z* isomer. The effect is less pronounced on the *E* isomer when the substitution is on the rotor phenyl group because of its twist out of the plane of the hydrazone core; 2) enhanced photoisomerization quantum yields are obtained when NMe_2 and NO_2 functional groups are introduced to the system; 3) derivatizing the rotor phenyl ring has less of an effect on thermal half-lives than substituting the stator phenyl ring; 4) EDGs at the stator phenyl group drastically accelerate the isomerization rate as a result of a hypothesized change in isomerization mechanism, whilst NO_2 at the non-coplanar rotor ring results in less significant acceleration; 5) push-pull systems can be used for red-shifting the absorption of both isomers while maintaining the bistability of the switch; and 6) charge transfer from *para*-NMe_2 at the rotary ring is important for efficient emission.

The analysis of the crystal structures of the *Z* isomers shed light on the solid-state packing-dependency of the switching performance, as well as the emission and quenching of the hydrazones in the solid-state. According to this analysis, we found that: 1) the presence of the twisted (out of plane) rotary phenyl ring in the hydrazone (Figure S88 in the Supporting Information) is crucial as it prevents, in general, the systems from stacking effectively, which results in the emergence of solid-state emission and efficient solid-state photoswitching; 2) nitro-substitution at the stator phenyl ring is detrimental to solid-state emission as it results in head-to-tail arrangement and quenching; 3) hydrazone **1** is not emissive in the solid-state indicating that EDGs and/or EWGs are required for the hydrazones to be emissive in the solid-state; 4) the enhancement of emission in the solid-state *vs* solution indicates that rigidification is responsible for the observed phenomenon.[27]

The insights of this study lay the ground for engineering hydrazone photochromic compounds with specific functions and properties derived from appropriate derivatization(s) of the rotor and/or stator phenyl groups. We are certain that these design principles will guide practitioners in their efforts to incorporate these photochromic compounds in a myriad of applications, including but not limited to data storage, [30] smart materials, [31] molecular machines, [32] photopharmacology,[8] and super-high resolution fluorescence microscopy, [33] among others.[34]

ASSOCIATED CONTENT

Supporting Information

The Supporting Information is available free of charge on ACS Publications website at DOI: http://pubs.acs.org.
General methods, experimental procedures, NMR spectra of key compounds, photoisomerization and kinetic studies, solution and solid-state emission studies (PDF)
Crystallographic data for **1**-*Z* (CIF)
Crystallographic data for **5**-*Z* (CIF)
Crystallographic data for **6**-*Z* (CIF)
Crystallographic data for **7**-*Z* (CIF)
Crystallographic data for **8**-*Z* (CIF)
Crystallographic data for **9**-*Z* (CIF)
Crystallographic data for **10**-*Z* (CIF)

AUTHOR INFORMATION

Corresponding Author

* ivan.aprahamian@dartmouth.edu

Author Contributions

†These authors contributed equally to this work.

Notes

The authors declare no competing financial interest.

ACKNOWLEDGMENT

We are grateful to the NSF (CHE-1807428) for the generous support. We gratefully acknowledge Prof. Richard Staples (Michigan State University) for X-ray data.

REFERENCES

(1) Harris, J. D.; Moran, M. J.; Aprahamian, I. New Molecular Switch Architectures. *Proc. Natl. Acad. Sci. U. S. A.* **2018**, *115*, 9414–9422.

(2) Bandara, H. M. D.; Burdette, S. C. Photoisomerization in different classes of azobenzene. *Chem. Soc. Rev.* **2012**, *41*, 1809–1825.

(3) Waldeck, D. H. Photoisomerization dynamics of stilbenes. *Chem. Rev.* **1991**, *91*, 415–436.

(4) Klajn, R. Spiropyran-based dynamic materials. *Chem. Soc. Rev.* **2014**, *43*, 148–184.

(5) Irie, M.; Fukaminato, T.; Matsuda, K.; Kobatake, S. Photochromism of Diarylethene Molecules and Crystals: Memories, Switches, and Actuators. *Chem. Rev.* **2014**, *114,* 12174–12277.

(6) Sluysmans, D.; Stoddart, J. F. Growing community of artificial molecular machinists. *Proc. Natl. Acad. Sci. U. S. A.* **2018**, *115*, 9359–9361.

(7) (a) Russew, M. M.; Hecht, S. Photoswitches: from molecules to materials. *Adv. Mater.* **2010**, *22*, 3348–3360; (b) Aida, T.; Meijer, E. W.; Stupp, S. I. Functional supramolecular polymers. *Science* **2012**, *335*, 813–817; (c) Lehn, J.-M. Perspectives in chemistry-aspects of adaptive chemistry and materials. *Angew. Chem. Int. Ed.* **2015**, *54*, 3276–3289.

(8) (a) Velema, W. A.; Szymanski, W.; Feringa, B. L. Photopharmacology: Beyond Proof of Principle. *J. Am. Chem. Soc.* **2014**, *136*, 2178–2191; (b) Broichhagen, J.; Frank, J. A.; Trauner, D. A Roadmap to Success in Photopharmacology. *Acc. Chem. Res.* **2015**, *48*, 1947–1960; (c) Lerch, M. M.; Hansen, M. J.; van Dam, G. M.; Szymanski, W.; Feringa, B. L. Emerging Targets in Photopharmacology. *Angew. Chem. Int. Ed.* **2016**, *55*, 10978–10999.

(9) (a) Stoll, R. S.; Hecht, S. Artificial light-gated catalyst systems. *Angew. Chem. Int. Ed.* **2010**, *49*, 5054–5075; (b) Blanco, V.; Leigh, D. A.; Marcos, V. Artificial switchable catalysts. *Chem. Soc. Rev.* **2015**, *44*, 5341–5370.

(10) (a) Molecular Switches; Feringa, B. L., Browne, W. R., Eds.; Wiley-VCH: Weinheim, Germany, **2011**. (b) Erbas-Cakmak, S.; Leigh, D. A.; McTernan, C. T.; Nussbaumer, A. L. Artificial Molecular Machines. *Chem. Rev.* **2015**, *115*, 10081–10206.

(11) Petermayer, C.; Dube, H. Indigoid Photoswitches: Visible Light Responsive Molecular Tools. *Acc. Chem. Res.* **2018**, *51*, 1153–1163.

(12) (a) Su, X.; Aprahamian, I. Hydrazone-based switches, metallo-assemblies and sensors. *Chem. Soc. Rev.* **2014**, *43*, 1963–1981; (b) Tatum, L. A.; Su, X.; Aprahamian, I. Simple Hydrazone Building Blocks for Complicated Functional Materials. *Acc. Chem. Res.* **2014**, *47*, 2141–2149; (c) Aprahamian, I. Hydrazone switches and things in between. *Chem. Commun* **2017**, *53*, 6674–6684.

(13) van Dijken, D. J.; Kovaříček, P.; Ihrig, S. P.; Hecht, S. Acylhydrazones as Widely Tunable Photoswitches. *J. Am. Chem. Soc.* **2015**, *137*, 14982–14991.

(14) (a) Yang, Y.; Hughes, R. P.; Aprahamian, I. Visible Light Switching of a BF_2-Coordinated Azo Compound. *J. Am. Chem. Soc.* **2012**, *134*, 15221–15224; (b) Yang, Y.; Hughes, R. P.; Aprahamian, I. Near-Infrared Light Activated Azo-BF_2 Switches. *J. Am. Chem. Soc.* **2014**, *136*, 13190-13193; (c) Qian, H.; Wang, Y.-Y.; Guo, D.-S.; Aprahamian, I. Controlling the Isomerization Rate of an Azo-BF_2 Switch Using Aggregation. *J. Am. Chem. Soc.* **2017**, *139*, 1037–1040.

(15) Crespi, S.; Simeth, N. A.; König, B. Heteroaryl azo dyes as molecular photoswitches. *Nat. Rev. Chem.* **2019**, *3*, 133–146.

(16) Hatano, S.; Horino, T.; Tokita, A.; Oshima, T.; Abe, J. Unusual Negative Photochromism via a Short-Lived Imidazolyl Radical of 1,1'-Binaphthyl-Bridged Imidazole Dimer. *J. Am. Chem. Soc.* **2013**, *135*, 3164–3172.

(17) (a) Helmy, S.; Leibfarth, F. A.; Oh, S.; Poelma, J. E.; Hawker, C. J.; Read de Alaniz, J. Photoswitching Using Visible Light: A New Class of Organic Photochromic Molecules. *J. Am. Chem. Soc.* **2014**, *136*, 8169–8172; (b) Lerch, M. M.; Szymanski, W.; Feringa, B. L. The (photo)chemistry of Stenhouse photoswitches: guiding principles and system design. *Chem. Soc. Rev.* **2018**, *47*, 1910–1937; (c) Mallo, N.; Foley, E. D.; Iranmanesh, H.; Kennedy, A. D. W.; Luis, E. T.; Ho, J.; Harpera, J. B.; Beves, J. E. Structure–function relationships of donor–acceptor Stenhouse adduct photochromic switches. *Chem. Sci.* **2018**, *9*, 8242–8252.

(18) (a) Su, X.; Lessing, T.; Aprahamian, I. The Importance of the Rotor in Hydrazone-Based Molecular Switches. *Beilstein J. Org. Chem.* **2012**, *8*, 872-876; (b) Tatum, L. A.; Foy, J. T.; Aprahamian, I. Waste management of chemically activated switches: using a photoacid to eliminate accumulation of side products. *J. Am. Chem. Soc.* **2014**, *136*, 17438–17441; (b) Foy, J. T.; Ray, D.; Aprahamian, I. Regulating signal enhancement with coordination-coupled deprotonation of a hydrazone switch. *Chem. Sci.* **2015**, *6*, 209–213; (c) Qian, H.; Aprahamian, I. An emissive and pH switchable hydrazone-based hydrogel. *Chem. Commun.* **2015**, *51*, 11158–11161; (d) Pramanik, S.; Aprahamian, I. Hydrazone Switch-Based Negative Feedback Loop. *J. Am. Chem. Soc.* **2016**, *138*, 15142–15145

(19) (a) Qian, H.; Pramanik, S.; Aprahamian, I. Photochromic Hydrazone Switches with Extremely Long Thermal Half-Lives. *J. Am. Chem. Soc.* **2017**, *139*, 9140–9143; (b) Li, Q.; Qian, H.; Shao, B.; Huges, R. P.; Aprahamian, I. Building Strain with Large Macrocycles and Using It to Tune the Thermal Half-Lives of Hydrazone Photochromes. *J. Am. Chem. Soc.* **2018**, *140*, 11829–11830.

(20) Ryabchun, A.; Li, Q.; Lancia, F.; Aprahamian, I.; Katsonis, N. Shape-Persistent Actuators from Hydrazone Photoswitches. *J. Am. Chem. Soc.* **2019**, *141*, 1196–1200.

(21) Moran, M. J.; Magrini, M.; Walba, D. M.; Aprahamian, I. Driving a Liquid Crystal Phase Transition Using a Photochromic Hydrazone. *J. Am. Chem. Soc.* **2018**, *140*, 13623–13627.

(22) Shao, B.; Baroncini, M.; Qian, H.; Bussotti, L.; Di Donato, M.; Credi, A.; Aprahamian, I. Solution and Solid-State Emission Toggling of a Photochromic Hydrazone. *J. Am. Chem. Soc.* **2018**, *140*, 12323−12327.

(23) The N−C single bond connecting the stator phenyl ring with the hydrazone backbone in **7** is shorter (1.380 Å) than the one found in **1** (1.403 Å) and **6** (1.393 Å) supporting this assessment (Figure S87 in the Supporting Information).

(24) This wavelength was used as it is the lower limit of the capability of our irradiation system.

(25) (a) Grabowski, Z. R.; Rotkiewicz, K.; Retting, W. Structural Changes Accompanying Intramolecular Electron Transfer: Focus on Twisted Intramolecular Charge-Transfer States and Structures. *Chem. Rev.* **2003**, *103*, 3899−4031; (b) Sasaki, S.; Drummen, G. P. C.; Konishi, G. Recent advances in twisted intramolecular charge transfer (TICT) fluorescence and related phenomena in materials chemistry. *J. Mater. Chem. C* **2016**, *4*, 2731−2743.

(26) (a) T. Förster, Excimers. *Angew. Chem. Int. Ed.* **1969**, *8*, 333−343; (b) Birks, J. B. Photophysics of Aromatic Molecules; Wiley: London, **1970**.

(27) Mei, J.; Leung, N. L. C.; Kwok, R. T. K.; Lam. J. W. Y.; Tang, B. Z. Aggregation-Induced Emission: Together We Shine, United We Soar! *Chem. Rev.* **2015**, *115*, 11718−11940.

(28) (a) Smets, G. Photochromic phenomena in the solid phase. *Advan. Polym. Sci.* **1983**, *50*, 17−44; (b) Naito, T.; Horie, K.; Mita, I. Photochemistry in polymer solids. 11. The effects of the size of reaction groups and the mode of photoisomerization on photochromic reactions in polycarbonate film. *Macromolecules* **1991**, *24*, 2907−2911.

(29) Mayerhöfer, T. G.; Mutschke, H.; Popp, J. Employing Theories Far beyond Their Limits-The Case of the (Boguer-) Beer-Lambert Law. *ChemPhysChem* **2016**, *17*, 1948−1955.

(30) (a) Kawata, S.; Kawata, Y. Three-Dimensional Optical Data Storage Using Photochromic Materials. *Chem. Rev.* **2000**, *100*, 1777−1788.

(31) (a) Roy, D.; Cambre, J. N.; Sumerlin, B. S. Future perspectives and recent advances in stimuli-responsive materials. *Prog. Polym. Sci.* **2010**, *35*, 278−301; (b) Ruskowitz, E. R.; DeForest, C. A. Photoresponsive Biomaterials for Targeted Drug Delivery and 4D Cell Culture. *Nat. Rev. Mater.* **2018**, *3*, 17087.

(32) Leigh, D. A.; Marcos, V.; Nalbantoglu, T.; Vitorica-Yrezabal, I. J.; Yasar, F. T.; Zhu, X. Pyridyl-Acyl Hydrazone Rotaxanes and Molecular Shuttles. *J. Am. Chem. Soc.* **2017**, 139, 7104−7109.

(33) (a) Huang, B.; Bates, M.; Zhuang, X. Super-resolution fluorescence microscopy. *Annu. Rev. Biochem.* **2009**, *78*, 993−1016; (b) Sydor, A. M.; Czymmek, K. J.; Puchner, E. M.; Mennella, V. Super-Resolution Microscopy: From Single Molecules to Supramolecular Assemblies. *Trends Cell Bio.* **2015**, *21*, 730−748; (c) Sahl, S. J.; Hell, S. W.; Jakobs, S. Fluorescence nanoscopy in cell biology. *Nat. Rev. Mol. Cell Biol.* **2017**, *18*, 685−701.

(34) Lutz, J. F.; Lehn, J. M.; Meijer, E. W.; Matyjaszewski, K. From precision polymers to complex materials and systems. *Nat. Rev. Mater.* **2016**, *1*, 16024−16027.